






Dynamics of all-optical single-shot switching of magnetization in Tb/Co multilayers

K. Mishra ¹, T. G. H. Blank ^{1,2}, C. S. Davies ³, L. Avilés-Félix ⁴, D. Salomoni ⁴, L. D. Buda-Prejbeanu ⁴, R. C. Sousa ⁴,
I. L. Prejbeanu ⁴, B. Koopmans ², Th. Rasing ¹, A. V. Kimel ¹, and A. Kirilyuk ^{3,*}

¹Radboud University, Institute for Molecules and Materials, Heyendaalseweg 135, 6525 AJ Nijmegen, The Netherlands

²Department of Applied Physics, Eindhoven University of Technology, P.O. Box 513, 5600 MB Eindhoven, The Netherlands

³FELIX Laboratory, Radboud University, Toernooiveld 7, 6525 ED Nijmegen, The Netherlands

⁴University Grenoble Alpes, CNRS, CEA, Grenoble INP, SPINTEC, 38000 Grenoble, France



(Received 17 February 2023; revised 25 April 2023; accepted 15 May 2023; published 14 June 2023)

Recent works have shown that the magnetization of Tb/Co multilayers can be switched all-optically by a single ultrashort laser pulse. Surprisingly, the same process cannot be achieved in TbCo alloys. Here, we present a plausible explanation for this difference in behavior based on the known treatment of angular momenta and the associated gyromagnetic ratio of rare-earth-based ferrimagnets. We then study in detail the composition-dependent dynamic behavior of the switching process in Tb/Co multilayers using single-shot time-resolved pump-probe experiments. We show that the observed dynamics is strongly dependent on the excitation fluence and multilayer composition and does not fit into the accepted framework describing the single-shot switching process found in Gd-based systems and Mn-containing Heusler alloys.

DOI: [10.1103/PhysRevResearch.5.023163](https://doi.org/10.1103/PhysRevResearch.5.023163)

I. INTRODUCTION

The recent spurt of developments in fields such as artificial intelligence, big data, and cloud-based technologies exerts significant pressure on our capacity to handle information, the majority of which is stored magnetically. Any new technology offering a superior means to write and preserve digital data must have a high bit density and read-write speed while also being energy efficient and sustainable. A promising route toward meeting all these criteria is offered by the phenomenon of helicity-independent all-optical switching (AOS): magnetization reversal driven by ultrashort laser pulses. This process was observed in amorphous ferrimagnetic alloys of GdFeCo [1], whereby the magnetization toggles between two oppositely oriented states following each single shot of a femtosecond laser pulse. Such single-shot toggle-switching has since been observed in other ferrimagnetic rare-earth transition-metal (RE-TM) alloys and multilayers, as well as the RE-free Heusler alloy Mn₂Ru_xGa [2–7]. The possibility of achieving this behavior in a robust medium suitable for high-density magnetic storage was opened with the observation of laser-induced magnetic nanostructures as small as 150 nm in a TbFe alloy film [8]. Recently, observations of single-shot switching in Tb-containing materials have been reported in Refs. [5–7]. These observations are particularly interesting since they have suggested that the switching process found in

Tb/Co multilayers is very distinct compared with that found in TbCo alloys as well as all other materials that show single-shot switching.

A critically important point that is not yet understood relates to why the single-shot switching typically found in the Gd-based RE-TM alloys seems to vanish when the gadolinium is replaced with terbium. Despite theoretical predictions of potential single-shot switching behavior [9], only a multishot helicity-dependent AOS (HD-AOS) has been experimentally found so far in Tb-based RE-TM alloys [10–14]. Intriguingly, the switching in the latter seems to resemble that found in ferromagnetic Co/Pt multilayers or FePt alloys. Recent experiments have revealed that RE-TM alloys containing a mixture of Tb and Gd, however, still display single-shot switching [5]. Indeed, in thin films of composition (Gd_xTb_{100-x})₂₂Co₇₈, single-shot switching persisted even when the concentration of Gd was reduced to just $x = 4\%$, whereas $x = 0\%$ led to its complete loss. This striking behavior was rationalized in Ref. [5] as stemming from differences in the element-specific damping of Tb and Gd. Contrary to these observations, single-shot switching has been identified in multilayered stacks of Tb/Co, with layer thicknesses on the order of nanometers [6,7]. The switching found in Tb/Co is rather robust, being achievable with a wide range of laser pulse durations and starting temperatures and persisting even when the multilayered stack is coupled with a CoFeB electrode to form a magnetic tunnel junction [7].

When closely comparing the process of single-shot switching displayed by Tb/Co multilayers with that displayed by all the other systems, one can identify an important difference involving the dependence of switching on the magnetization compensation temperature T_{comp} . This is the characteristic temperature of a ferrimagnet at which the sublattice magnetic moments compensate each other, resulting in zero net

*Corresponding author: andrei.kirilyuk@ru.nl

Published by the American Physical Society under the terms of the [Creative Commons Attribution 4.0 International](https://creativecommons.org/licenses/by/4.0/) license. Further distribution of this work must maintain attribution to the author(s) and the published article's title, journal citation, and DOI.

magnetization. Single-shot switching at room temperature (RT) in $\text{Mn}_2\text{Ru}_x\text{Ga}$ alloys is only seen in compositions with $T_{\text{comp}} > \text{RT}$ [15], whereas Gd-based RE-TM systems such as GdFeCo alloys, Gd/Co bilayers, and Gd/FeCo multilayers show single-shot switching on either side of T_{comp} [2,16,17]. These dependencies have already been unified under a common framework proposed by Davies *et al.* [15,18,19]. The reversal dynamics were described in terms of the interplay of three kinds of relaxation processes: (i) ultrafast and independent demagnetization of the two sublattices, dictated by the sublattice-specific magnetic moment and damping; (ii) demagnetization with conservation of spin angular momentum, governed by the exchange interaction between the sublattices; and (iii) slower changes after the sublattices attain a common temperature and the magnetizations of both sublattices are in equilibrium with the lattice temperature. The parameters governing this interplay are the pulse width of the excitation, the temperature dependence of magnetization, the value of T_{comp} relative to the temperature of the film prior to excitation, the electronic structure at the Fermi level, and intersublattice exchange coupling. In stark contrast, switching of magnetization in Tb/Co multilayers at RT has only been found in compositions with $T_{\text{comp}} < \text{RT}$ [6]. This has not yet been rationalized within the aforementioned framework. To therefore understand how the single-shot switching in Tb/Co fits in relation to the generalized framework of single-shot switching in these other systems, the magnetization dynamics must be analyzed in detail.

Here, we present a plausible hypothesis to explain why Tb-containing RE-TM alloys do not display single-shot switching, whereas Tb/Co multilayers do. We revisit early discussions of how the crystal fields and spin-orbit interactions control the angular momentum of RE elements in ferrimagnets [20–22] and argue that it is the difference in atomic environment of Tb in the alloys and multilayers that makes the critical difference. Namely, the strong crystal field in alloys quenches the dynamic part of the angular momentum of Tb, thus removing the reservoir necessary for switching via the exchange-driven mechanism found in GdFeCo and $\text{Mn}_2\text{Ru}_x\text{Ga}$ alloys [19].

To make first steps toward exploring the validity of this hypothesis, we experimentally study the spatiotemporal process of single-shot switching of magnetization displayed in various Tb/Co multilayer compositions using pump-probe spectroscopy and single-shot time-resolved magneto-optical imaging. We identify key differences in the temporal dependence of the switching process involved in Tb/Co multilayers and all the other systems, i.e., Gd-based RE-TM alloys and multilayers, and $\text{Mn}_2\text{Ru}_x\text{Ga}$ alloys. The switched magnetic state in Tb/Co stabilizes on a time scale of ~ 50 – 100 ps after the laser excitation, revealing a slower switching process than that associated with Gd-based alloys and multilayers, where the switched state stabilizes within a few picoseconds [17,23]. Time-resolved images show that the switching process involves the formation of ring-shaped magnetic textures, like signatures of precessional behavior, further highlighting the differences in the switching dynamics compared with previously studied materials. While not conclusive, our results suggest that the effective gyromagnetic ratio (which governs transversal magnetization dynamics) might play a role in the

process of all-optical magnetic switching found in Tb/Co multilayers.

II. Tb/Co MULTILAYERS VS TbCo ALLOYS: WHAT TO EXPECT?

Previous works have shown that the process of single-shot switching of magnetization is crucially dependent on the balance of angular momentum in the ferrimagnetic system [15,18]. From the experimental point of view, the magnetization compensation is directly indicated by the diverging coercive field in the static regime. In contrast, the angular momentum compensation only appears in dynamics, indicated by the increase of the effective gyromagnetic ratio of the ferrimagnetic system. It is the latter that really should be considered in the process of single-shot switching, as the process is fully dependent on the balance of the angular momentum of the sublattices [24]. Differences in the atomic environment of Tb in Tb-based alloys and multilayers, arising from the crystal field and spin-orbit coupling interactions, might possibly lead to significant differences in their effective gyromagnetic ratios. This, in turn, could affect both the angular momentum compensation point and the switching behavior, as rationalized below.

Approaches to calculate the effective gyromagnetic ratio γ_{eff} of a ferrimagnet were presented more than half a century ago by Wangsness [20], Kittel [21], and van Vleck [22]. For a ferrimagnet containing two magnetic sublattices, each with a magnetization M_i and gyromagnetic ratio γ_i ($i = 1, 2$), Wangsness [20] formulated a straightforward and seemingly logical approach such that [20]

$$\gamma_{\text{eff}} = \frac{M_1 + M_2}{\frac{M_1}{\gamma_1} + \frac{M_2}{\gamma_2}}. \quad (1)$$

This was shown by Wangsness [20] to provide a satisfactory description of resonances in nickel ferrite-aluminates. Later on, Kittel [21] suggested that, because of its strong relaxation, the highly damped RE sublattice within RE iron garnets should not be counted in the dynamic part of the angular momentum of the ferrimagnet, i.e., the RE sublattice fully contributes to the magnetization of the ferrimagnet but not to its angular momentum. Equation (1) therefore becomes [21]

$$\gamma_{\text{eff}} = \frac{M_{\text{Fe}} + M_{\text{RE}}}{\frac{M_{\text{Fe}}}{\gamma_{\text{Fe}}}}. \quad (2)$$

Equation (2) appears to reasonably describe the effective g factors reported for RE-containing iron-garnets containing Dy, Ho, and Er [21,25]. Moreover, Kittel [21] projected that Eq. (2) is relevant for describing the dynamics of ferrimagnetic materials containing two magnetic ions that have substantially disparate damping, with the notable exception of systems containing gadolinium since this RE element has zero orbital moment and thus interacts weakly with the environment.

In the subsequent work of van Vleck [22], the RE sublattice was treated as being subservient to the exchange field of iron while also having its energy levels split by crystalline fields and/or spin-orbit interactions. In the case of gadolinium iron garnet, the crystal field is negligible relative to the exchange

field, so the effective gyromagnetic ratio is well described by Eq. (1), i.e., with the angular momentum of both the Gd and Fe sublattices contributing to γ_{eff} . For the other RE elements, van Vleck [22] derives Eq. (2) on the basis that the gyromagnetic ratio of the RE sublattice vanishes on account of static crystalline fields, rather than highly damping spin-lattice interactions. While Kittel [21] and van Vleck [22] arrive at the same result from different starting points, the latter also admits that “in a certain sense, however, the difference between our theory and Kittel’s is a semantic one.” This is the reason why the simple and easy-to-understand qualitative formula of Kittel [21] is popular.

Note that these approaches have been confirmed by multiple studies examining the temperature dependence of ferromagnetic resonance (FMR) and domain-wall motion in RE-doped iron garnets. In Ref. [26], experimental measurements of the effective g factor in $(\text{La}, \text{Tm}, \text{Ca})_3(\text{Fe}, \text{Ga})_5\text{O}_{12}$ could only be explained when considering Eq. (2), i.e., when excluding the contribution of Tm. A similar conclusion was reached by Randoshkin *et al.* [27] with a study of the effective gyromagnetic ratio of $(\text{Gd}, \text{Tm}, \text{Bi})_3(\text{Fe}, \text{Ga})_5\text{O}_{12}$. The latter was further confirmed by the recent observation in Ref. [28] that the angular momentum compensation point of a very similar film exceeds that of the magnetization compensation. In addition, experimental works have reported that the effective g factor of $\text{Eu}_3\text{Fe}_5\text{O}_{12}$, $\text{Tm}_3\text{Fe}_5\text{O}_{12}$, $\text{Dy}_3\text{Fe}_5\text{O}_{12}$, and $\text{Dy}_x\text{Y}_{3-x}\text{Fe}_5\text{O}_{12}$ is also explained by Eq. (2) [29–31].

Considering the above, we construct a hypothesis to explain why RE-TM ferrimagnetic systems containing gadolinium can display single-shot switching, whereas those containing terbium do not. The strong spin-orbit coupling of terbium suggests that Eq. (2) is more appropriate in describing the effective g factor of Tb-based RE-TM alloys. Consequently, although Tb-based RE-TM alloys remain ferrimagnetic with a magnetization compensation point, they behave as simple ferromagnets from the point of view of angular momentum. Such ferromagneticlike dynamics of angular momentum gives rise to the HD multishot switching of magnetization as observed in Co/Pt and Co/Pd multilayers or in FePt alloys [11]. Completely distinct from single-shot switching, the HD-AOS exhibited by TbCo alloys stems either from the combined action of magnetic circular dichroism and local differential heating or from the inverse Faraday effect.

What is so different in the case of Tb/Co multilayers? In this case, Tb atoms are not encapsulated in a Co matrix such as in alloys, and the crystal fields are considerably weaker. In the case of pure Tb, there is a certain amount of crystal field interaction that overdamps the dynamics of the Tb spins. However, it affects the dynamics to a much lesser extent, which is indicated by a nontrivial behavior of FMR in Tb crystals: at high frequencies (~ 100 GHz), the spins behave rather independently from the lattice, and the resonance behaves in accordance with the model by Wangsness [20] [i.e., according to the frozen lattice approximation given by Eq. (1)] [32]. At low frequencies, in contrast, the spins are overdamped by the lattice, and the behavior of FMR becomes rather counterintuitive [33], following better the models of Kittel [21] and van Vleck [22] [see Eq. (2)]. As our experiments on single-shot switching correspond to frequencies of hundreds of gigahertz, Tb in the Tb/Co multilayered stacks behaves as expected,

with a nonzero contribution to the angular momentum. A more in-depth theoretical discussion of these free- or frozen-lattice models is given in Ref. [34].

Ultimate experimental verification of this hypothesis would involve determining the angular momentum compensation points in Tb-based systems for various alloy and multilayer compositions and subsequently correlating these points with the respective switching behavior. While this is beyond the scope of this paper, the proposed hypothesis highlights the need to explore the role of angular momentum and its compensation in Tb-based systems having a nontrivial separation between the magnetization and angular momentum compensation points. Toward this end, we therefore report the experimentally determined spatiotemporal dynamics of different multilayer compositions. Overall, we find that the process of AOS in Tb/Co features oscillations of the magnetization, suggesting that precessional motion may be involved. As such, our measurements reveal not only the highly dissimilar magnetization dynamics found in Tb-based RE-TM alloys compared with their multilayered counterparts but also suggest that the effective gyromagnetic ratio might play an important role.

III. MATERIALS AND METHODS

In our experiments, we study a 4-inch-diameter wafer of Tb/Co grown on a silicon substrate. The multilayered structure is of composition $[\text{Tb}(t_{\text{Tb}})/\text{Co}(t_{\text{Co}})]_5$ with graded thicknesses of the Tb and Co layers spanning $1 \text{ nm} < t_{\text{Tb}} < 1.8 \text{ nm}$ and $0.8 \text{ nm} < t_{\text{Co}} < 1.8 \text{ nm}$ [6]. The static magneto-optical images shown in the top row of Fig. 1(a), taken after exposing the sample to subsequent femtosecond laser pulses at RT, confirm that the multilayer composition $[\text{Tb}(1.2 \text{ nm})/\text{Co}(1.7 \text{ nm})]_5$ displays toggle switching. In contrast, the multilayer composition $[\text{Tb}(1.2 \text{ nm})/\text{Co}(0.9 \text{ nm})]_5$ displays only thermally induced demagnetization [bottom row of Fig. 1(a)]. Figure 1(b) shows the spatial variation of the coercive field across the sample as mapped by Avilés-Félix *et al.* [6], with the strength of the coercive field indicated on the adjacent color scale. The gray-shaded region along the diagonal of the wafer indicates a coercive field that is too high to be measured by our experimental setup. In this region, the moments of Tb and Co begin to compensate each other, leading to an increasingly antiferromagneticlike behavior characterized by diverging coercive fields and net zero magnetization. The Tb and Co layer thicknesses along the diagonal of the wafer correspond to compositions having a magnetization compensation point close to RT, i.e., $T_{\text{comp}} \sim \text{RT}$. Moving away from the diagonal, the Co (Tb)-rich compositions instead have a magnetization compensation point below (above) RT.

We measured the magnetization dynamics for different multilayer compositions using pump-probe spectroscopy with a pump (probe) of central wavelength 800 nm (650 nm). Both pump and probe beams were derived from an amplified Ti:sapphire laser system with a repetition rate of 1 kHz and were focused on the sample surface to average spot radii of 35 and 19 μm , respectively, with variation within $\pm 4 \mu\text{m}$ between measurements on different sample compositions. The probe was obtained by optical parametric amplification of the 800-nm laser output. The pump was incident at an angle of

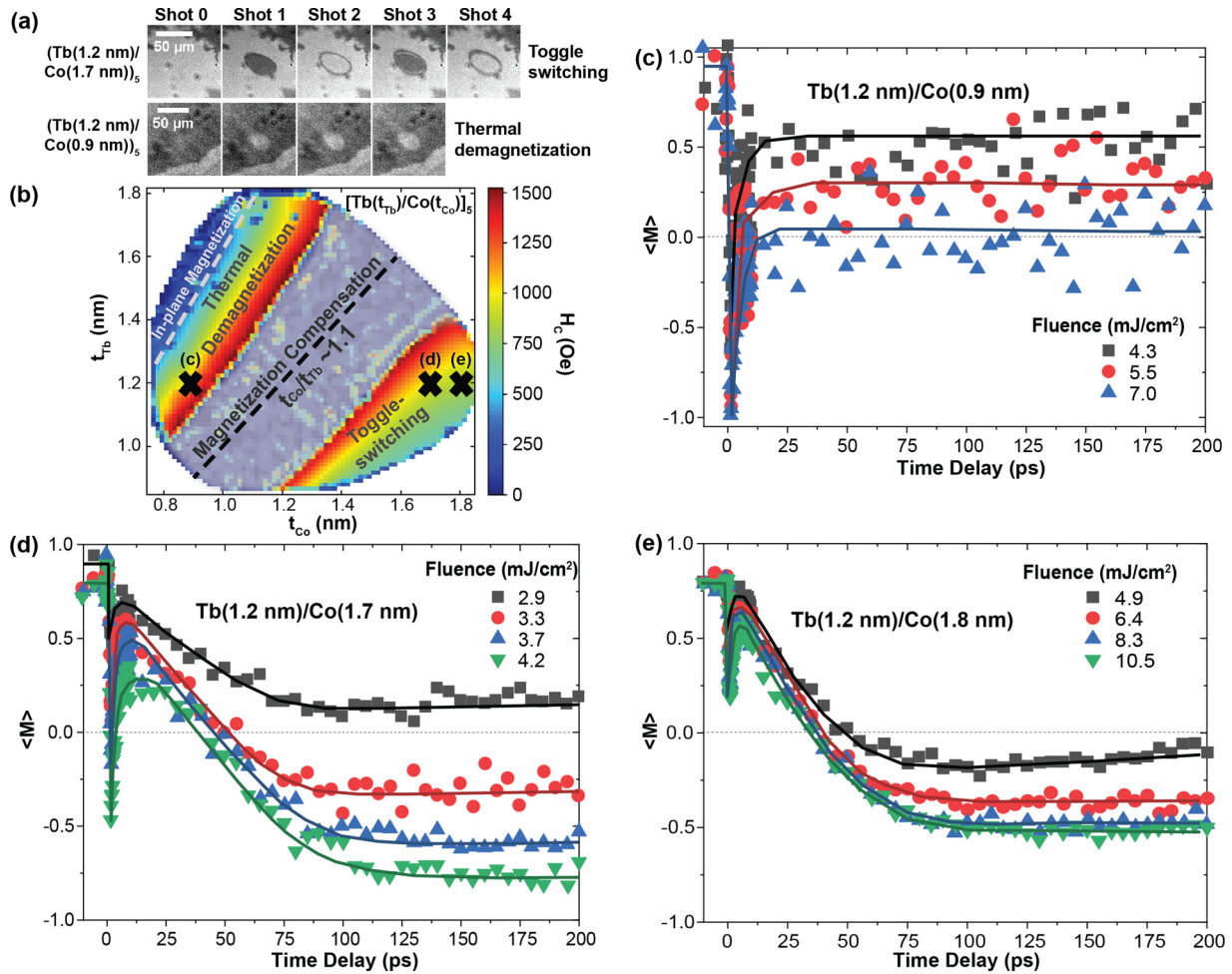


FIG. 1. (a) Static magneto-optical images taken after exposing multilayered stacks of Tb/Co to subsequent femtosecond laser pulses at room temperature, as indicated. (b) Dependence of the coercive field H_c of the Tb/Co multilayered sample on the thickness of the layers t (adapted from Ref. [6]). The Tb-rich region shows thermal demagnetization in response to a laser pulse, whereas the Co-rich region shows toggle switching; (c)–(e) Calibrated magnetization dynamics measured for (c) $[\text{Tb}(1.2 \text{ nm})/\text{Co}(0.9 \text{ nm})]_5$ showing laser-induced thermal demagnetization; (d) $[\text{Tb}(1.2 \text{ nm})/\text{Co}(1.7 \text{ nm})]_5$ showing single-shot switching; and (e) $[\text{Tb}(1.2 \text{ nm})/\text{Co}(1.8 \text{ nm})]_5$ with a thicker Co layer, also showing single-shot switching. The different points were measured with different incident pump fluences as indicated, and the solid lines are a guide to the eye.

$\sim 20^\circ$ to the sample normal. The probe was at near-normal incidence and hence sensitive to the out-of-plane component of magnetization of the multilayer sample. Throughout the entire pump-probe spectroscopic measurements, a constant magnetic field having strength higher than the coercive field for a given composition (ranging from 100 to 250 mT, depending on the composition) was applied to reinitialize the saturated magnetic state of the system before the arrival of the next pump pulse from the 1-kHz source.

To both calibrate the spectroscopic pump-probe measurements and to obtain spatial resolution of the switching process, time-resolved magneto-optical images were recorded using the same pump and probe pulses albeit delivered in a hardware-triggered single-shot mode. This approach involves the use of a single pair of pump and probe pulses to image the pump-induced magnetization contrast changes at each pump-probe time delay value. The triggering of the laser to fire the pump and probe pulse in turn triggers the camera to record an image. After recording each image, a reinitializing magnetic field, higher than the coercive field

of the composition, is applied. Magneto-optical images are recorded after the reinitialization and before the subsequent pump incidence to confirm the saturated state of the sample. Such a time-resolved single-shot measurement was repeated several times to allow the averaging over multiple frames. Although the single-shot nature of this technique lowers the signal-to-noise ratio compared with stroboscopic pump-probe measurements, such a configuration allows for waiting times of the order of seconds between two consecutive pump pulses. Thus, it effectively excludes any possibility of heat accumulation from a 1-kHz train of pulses. Furthermore, to exclude any precessional effects that could arise from an external magnetic field and to accurately establish the time scale of the switching process, single-shot imaging was performed under zero applied magnetic field at the time of the pump incidence and image recording. In a separate set of experiments, single-shot time-resolved imaging was also carried out in the presence of a continuously applied external magnetic field in both out-of-plane and in-plane configurations to gain a better understanding of the magnetic textures observed in the zero-

field geometry. As with the zero-field single-shot imaging, a reinitializing field, higher than the coercive field of each composition, was used to saturate the sample following each pump incidence, confirmed by recording magneto-optical images. Reference images corresponding to the two oppositely oriented saturated magnetization states, i.e., $\langle M \rangle \pm 1$, were recorded for each frame to calibrate the contrast to the average magnetization value. Further details of the experiments can be found in Ref. [35]. The large pulse-to-pulse fluctuation of the pulsed laser output led to an uncertainty of up to 10% in the calibration.

IV. RESULTS AND DISCUSSION

In this section, we discuss the experimental results disclosing the magnetization dynamics in Tb/Co multilayers as measured by pump-probe spectroscopic measurements (Sec. IV A), single-shot time-resolved imaging in the absence of a magnetic field (Sec. IV B), and under a continuously applied external magnetic field (Sec. IV C).

A. Pump-probe dynamics

Avilés-Félix *et al.* [6] previously characterized how T_{comp} and the switching behavior in Tb/Co multilayers depends on the nanolayer thickness, using static magneto-optical imaging. Multilayered Tb/Co stacks on the Co-rich side showed toggle switching, i.e., each subsequent laser shot switched the net magnetization of the affected area between the two opposite states with net magnetization ($\langle \mathbf{M} \rangle = \pm 1$). Samples on the Tb-rich side, in contrast, showed thermal demagnetization, i.e., a single laser pulse reduced the net magnetization $\langle \mathbf{M} \rangle$ of the affected region to zero, creating small randomized domains of both orientations. Each subsequent shot only randomized the domains further, and no homogeneous contrast reversal was observed. We investigated the magnetization dynamics of the multilayers for both Tb- and Co-rich compositions. Figures 1(c)–1(e) show the magnetization dynamics across a time scale of 200 ps, measured for three different compositions with a fixed Tb thickness and a varying thickness of the Co layer. All compositions show an ultrafast demagnetization occurring within 1 ps, followed by a fast partial recovery of magnetization within the next 10 ps. Beyond this point, the dynamics differ for the Tb- and Co-rich compositions. For the Tb-rich composition [Tb(1.2 nm)/Co(0.9 nm)] in Fig. 1(c), following a large ultrafast demagnetization within 1 ps, the magnetization eventually stabilizes to a constant positive value, corresponding to a partly demagnetized state. For the Co-rich compositions—namely, Tb(1.2 nm)/Co(1.7 nm) in Fig. 1(d) and Tb(1.2 nm)/Co(1.8 nm) in Fig. 1(e)—the fast partial recovery of magnetization is followed instead by a slower demagnetization step, which eventually stabilizes to a constant negative value after ~ 75 –100 ps (depending on the composition). This fixed final value represents a homogeneously switched magnetic state, which appears to stabilize faster for multilayered stacks with thicker Co layers. Upon increasing the pump fluence, an increase is observed in the degree of ultrafast demagnetization and, surprisingly, also the value of final magnetization. This can be explained by the possibil-

ity that higher pump fluences induce nonuniform magnetic textures. Since the probe spot has a radius on the order of ~ 20 μm , the measured signal integrates over spatially varying magnetization dynamics, leading to trends that can be counterintuitive.

The magnetization dynamics in the single-shot switching regime can thus be divided into three steps: (i) ultrafast demagnetization; (ii) fast, partial magnetization recovery, manifesting as an upturn in the detected signal; and (iii) slower change of magnetization, leading to an eventual stabilization to the switched state. Compared with the switching dynamics found in GdFeCo alloys and Gd/Fe bi-/multilayers, the main difference for the Tb/Co multilayer dynamics is the upturn observed in step (ii). A similar feature was reported by Mekonnen *et al.* [36] in the observed thermal demagnetization of GdFeCo and GdCo alloys, albeit these dynamics did not correspond to the scenario of single-shot switching. This behavior was rationalized using a four-temperature model, where the dynamics of the system was modeled based on thermal exchange between four reservoirs: electrons, lattice, Gd spins, and FeCo (or Co) spins. The observed upturn in GdCo and GdFeCo was attributed to intersublattice exchange between the two spin reservoirs. Varying the strength of the intersublattice coupling in this four-temperature model influenced both the gradient of the upturn and the ratio of the ultrafast demagnetization to the total degree of magnetization change. This feature and reasoning were later reproduced when examining the demagnetization dynamics of TbFeCo alloys as well [37]. The three-step process observed in the switching dynamics of the Tb/Co multilayers therefore appears like that observed in GdFeCo samples, while also occurring across similar time scales [36]. The ratio between the ultrafast initial change in the Tb/Co magnetization to the total change in the magnetization at the end of the switching seems to show a dependence on the Co layer thickness. However, intersublattice coupling is expected to be much weaker in multilayers, as the RE-TM contact area is limited to the interfaces, unlike for alloys. Thus, changing the Co layer thickness is not expected to affect the intersublattice coupling since the number of interfaces remain fixed. Hence, the dynamics in the multilayers cannot be adequately explained using the notion of intersublattice coupling arising from such a four-temperature model. The fast and slow relaxation times were extracted from the dynamics for all compositions, but no dependence was observed on either composition or fluence.

B. Single-shot imaging dynamics

To spatially resolve the switching dynamics and to reliably calibrate the magnetic state at a given time, single-shot time-resolved magneto-optical images were recorded up to a time scale of 2 ns. In Fig. 2, representative images acquired for selected time delays are shown, highlighting the most important spatial features. Figures 2(a)–2(c) show the dynamics for the same three multilayer compositions as indicated in Figs. 1(c)–1(e), respectively. Each panel shows a background-subtracted image, obtained by subtracting magneto-optical images taken before and after the excitation event. Thus, only laser-induced magneto-optical contrast changes are shown at the different time delays.

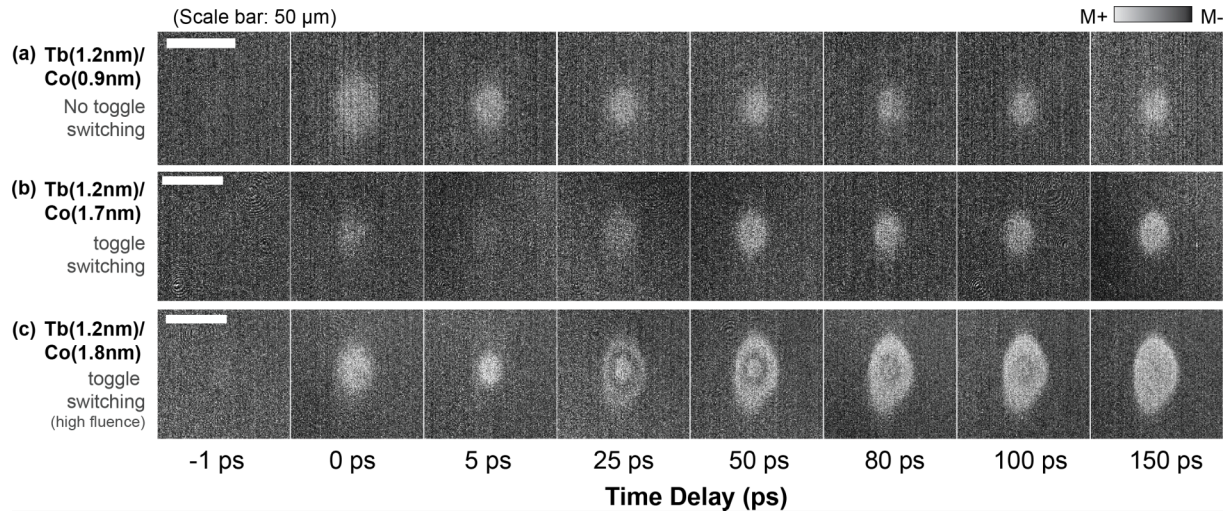


FIG. 2. (a)–(c) Time-resolved magneto-optical images of single-shot switching recorded at different pump-probe delays as indicated. The images in rows (a)–(c) correspond to different multilayer compositions and pump fluences, with (a) Tb(1.2 nm)/Co(0.9 nm), pump fluence 3.6 mJ/cm^2 ; (b) Tb(1.2 nm)/Co(1.7 nm), pump fluence 3.6 mJ/cm^2 ; and (c) Tb(1.2 nm)/Co(1.8 nm), pump fluence 10.1 mJ/cm^2 . Pure thermal demagnetization is seen in row (a), whereas single-shot switching is seen in rows (b) and (c).

From the images shown in Fig. 2, the differences between thermal demagnetization and single-shot switching become quite apparent. For the composition Tb(1.2 nm)/Co(0.9 nm) in Fig. 2(a), showing thermal demagnetization, the magnetic contrast changes from a dark saturated background (at -1 ps) to the ultrafast appearance of a spot with brighter contrast (at 0 ps). Following this, the laser-induced spot seems to retain the same contrast although its area decreases and its edges become better defined. This is consistent with the pump-probe traces from the previous section, comprising a three-step process of ultrafast demagnetization, partial relaxation, and eventual stabilization at a constant value in the original direction. The images in Fig. 2(a) are shown for a pump fluence of 3.6 mJ/cm^2 , remaining qualitatively similar even as the pump fluence is varied.

For the compositions Tb(1.2 nm)/Co(1.7 nm) in Fig. 2(b) and Tb(1.2 nm)/Co(1.8 nm) in Fig. 2(c), the switching behavior is shown for a low (3.6 mJ/cm^2) and high (10.1 mJ/cm^2) pump fluence, respectively. In both cases, an initial contrast change is observed at the moment of laser incidence (0 ps), like that observed in Tb(1.2 nm)/Co(0.9 nm). For the case of low-fluence excitation, this is followed by an initial reduction of the laser-induced contrast change and then an increase starting at $\sim 25 \text{ ps}$ until eventually a homogeneous switched spot is stabilized at $\sim 100 \text{ ps}$, resembling the dynamics trace. For the case of high-fluence excitation, shown in Fig. 2(c), ring-shaped magnetic textures emerge within the time interval between the initial laser-induced magnetic contrast changes and the final stabilization of a homogeneous switched spot at $\sim 150 \text{ ps}$. The central area of the total laser-affected spot retains the initial bright contrast change throughout, whereas the contrast change reduces in the outer area, bringing it closer to its initial magnetization. Following this, at $\sim 20\text{--}25 \text{ ps}$ [35], the outer ring of the laser-affected spot regains a brighter contrast but is separated from the central bright area by a ring of opposite, darker contrast. This separation gradually disappears at $\sim 100 \text{ ps}$, and the entire

spot attains a uniform bright contrast, corresponding to the homogeneously switched state. This corroborates our discussion of Sec. II that, unlike the case of alloys, Tb/Co multilayers can be switched with single laser pulses. We observe from this dataset, however, that the switched state in Tb/Co multilayers stabilizes on a time scale of 100 ps , much slower than in GdFeCo alloys [23], Gd/Fe bilayers [17], or $(\text{Gd/Fe Co})_{20}$ multilayers [2], where the switching stabilized within a few picoseconds.

The inhomogeneous spatial dynamics of magnetization underpinning the single-shot switching process in Tb/Co multilayers substantially differs from that found in Gd-based systems. In the latter, no ringlike textures have been observed in the absence of an applied magnetic field [2,38]. The emergence of these ring textures with increasing fluence is visualized more clearly in Figs. 3(a)–3(c), showing the time-resolved behavior of magnetization in Tb(1.2 nm)/Co(1.7 nm) as recorded for three pump fluence values, increasing from 3.6 to 10.1 mJ/cm^2 .

To quantify and calibrate laser-induced magnetization changes from the time-resolved images, the pixel contrast value, or gray value, was extracted from the magneto-optical images. Reference magneto-optical images of the two opposite saturated magnetic states were recorded to define the gray value corresponding to the magnetization states with $\langle M \rangle = \pm 1$, and a linear relationship was used to calibrate the intermediate $\langle M \rangle$ values. Applying the calibration within an appropriate region of interest (ROI) yielded time traces of the magnetization dynamics which look like those obtained by pump-probe dynamics measurements. Such traces are shown in Figs. 4(a)–4(d), where the single-shot switching behavior in different compositions at various pump fluences has been quantified for different ROIs within the laser-affected spot.

Figures 4(a)–4(c) show the magnetization dynamics extracted from the imaging experiments for a sample of composition Tb(1.2 nm)/Co(1.7 nm), measured with three different excitation fluences. Since no inhomogeneous

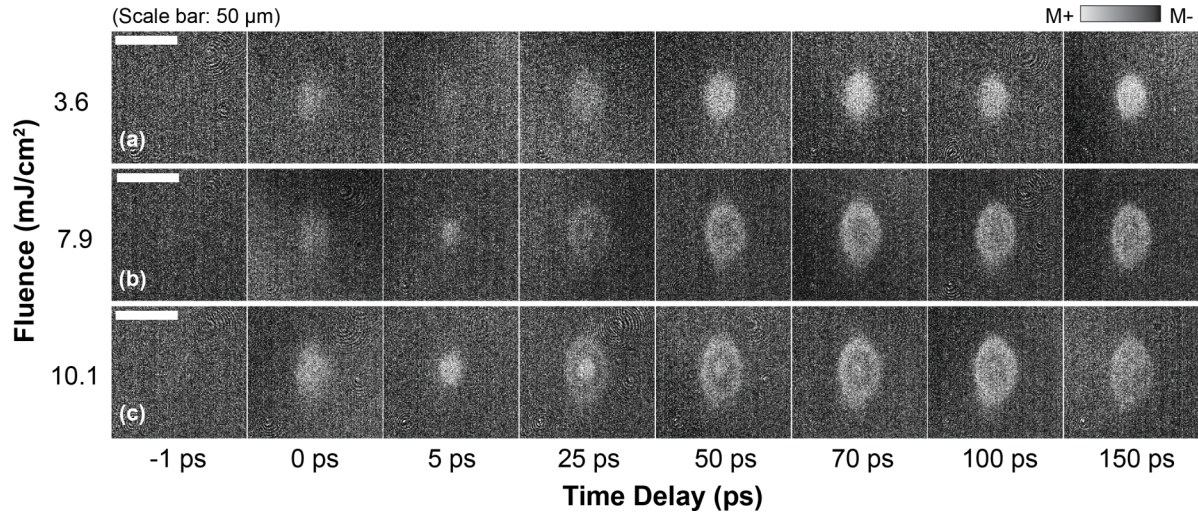


FIG. 3. Time-resolved magneto-optical images showing the temporal evolution of the single-shot switching process for incident pump fluences of (a) 3.6 mJ/cm², (b) 7.9 mJ/cm², and (c) 10.1 mJ/cm². The dynamics were recorded for the multilayered stack of composition Tb(1.2 nm)/Co(1.8 nm), in the absence of an external magnetic field.

magnetic textures were observed within the switched spot for the lowest incident fluence in Figs. 3(a) and 4(a), we defined two ROIs: a small area at the center of the switched spot and the entire switched spot. The averaged dynamics within both ROIs are identical, implying that homogeneous reversal

takes place close to the single-shot switching threshold within a spatial resolution of ~2 μm. At the higher pump fluences shown in Figs. 3(b) and 3(c) and Figs. 4(b) and 4(c), inhomogeneous magnetic textures are observable. We define ROIs that separate the laser-affected area into regions with different

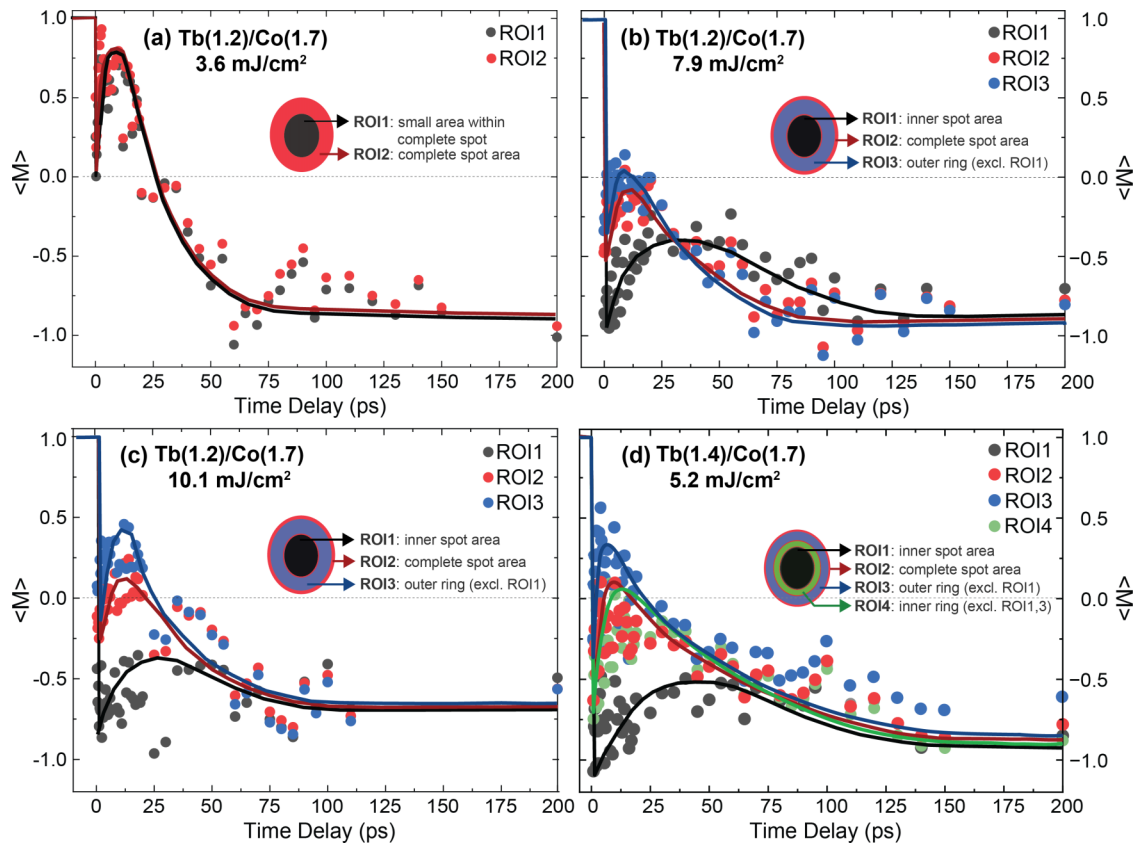


FIG. 4. (a)–(d) Traces of magnetization dynamics extracted from the time-resolved magneto-optical images for Tb/Co samples with different compositions and pump fluences as indicated. The inset of each plot indicates the selected regions of interest (ROIs). The solid lines are a guide to the eye.

temporal evolution of magnetization, as shown schematically in the insets of the respective plots in Figs. 4(b) and 4(c). ROIs are also defined over the entire spot, representing the spatially averaged dynamics measured by the probe in the pump-probe dynamics experiments discussed in the previous section (see also the Appendix). The center of the laser-excited region shows the strongest ultrafast demagnetization and, in some cases, switching. For ROIs further from the center, the degree of ultrafast demagnetization decreases with the distance from the center. This is expected for a laser pulse with a Gaussian intensity profile, for which the effective fluence decreases when moving away from the spot center, thus causing less demagnetization. The difference between the degree of ultrafast demagnetization of the central spot and the outer ring grows as the incident fluence is increased. For all the ROIs, the initial ultrafast demagnetization is followed by a fast, partial magnetization recovery. As expected from Refs. [39,40], the region with the largest demagnetization, i.e., the central spot, shows the slowest relaxation. The relaxation is followed by a slower change in magnetization, and eventually, after ~ 100 ps, the dynamics for all the ROIs converge and homogeneous switching is attained.

Figure 4(d) shows the spatially resolved magnetization dynamics for the composition Tb(1.4 nm)/Co(1.7 nm). While changing the multilayer composition quantitatively influences the amount and time scale of the demagnetization, the overall behavior is qualitatively unaffected. For Fig. 4(d), the ROIs are defined as the central spot, the outermost ring, and the ring of opposite contrast that separates the latter two regions. At the central spot, the ultrafast demagnetization (and switching) is at its strongest and fastest. Upon moving further from the center, the demagnetization becomes more gradual in both its strength and speed.

The transient ringed texture might possibly originate from magnetization precession. A similar bull's-eye-shaped magnetic structure was reported by Davies *et al.* [41] in dielectric Bi-substituted yttrium-iron-garnet (Bi:YIG), which arose from external magnetic-field-induced precession following the pump excitation. In that case, the Gaussian intensity profile of the pump beam created a radial gradient that thermally modified the crystalline anisotropy across the laser-excited region. Spins at different points along this gradient experienced different effective magnetic fields and accordingly precessed for either odd or even half-periods, resulting in alternating well-defined rings of bright and dark contrast. There are two important differences between these textures observed in Bi:YIG and Tb/Co. First, in Tb/Co multilayers, the ringed textures are observed in the absence of any external magnetic field applied in the plane of the sample. Magnetic precession is therefore not expected in Tb/Co due to its perpendicular magnetic anisotropy, as confirmed in polar Kerr hysteresis loops (not shown) and RT superconducting quantum interference device (SQUID) measurements (shown in the Appendix). Second, unlike Bi:YIG, which eventually stabilizes to an equilibrium magnetic state retaining the bull's eye texture, the ringed texture in Tb/Co multilayers collapses to a homogeneously reversed state. Although the magnetic anisotropy in the dielectric Bi:YIG has different origins and temperature dependence compared with that of the metallic Tb/Co multilayers, the ringed textures could nevertheless hint

at precessional dynamics being involved in the single-shot switching observed in Tb/Co.

An important point that needs to be discussed here relates to the strong overshoot of the measured magneto-optical signal across the time scale of 0–1 ps. In some cases, this overshoot even reaches the value corresponding to the oppositely saturated magnetization [see Figs. 4(b)–4(d)]. This is followed by a considerable relaxation, even crossing the zero line again. Given the very short time scale, we rule out a precessional mechanism underpinning this overshoot and instead tentatively ascribe it to the longitudinal dynamics. Note that, in Ref. [42], the magnetization of the TM sublattice was also shown to cross zero across a subpicosecond time scale, with subsequent relaxation to the initial state. On the other hand, such a structure with subnanometer-scale inhomogeneities may lead to very strong local spin-polarized currents [43], which could have a considerable effect on the detected magneto-optical signals. In the case of a heterogeneous multilayer structure, such as the case in this paper, the inhomogeneity across the thickness is much more sizeable than the randomized variation of concentration considered in Ref. [43]. It is thus important to consider this. To prove the existence of either behavior, however, x-ray-based element-resolved measurements of the switching dynamics are required [35].

C. Dynamics under applied magnetic field

To attempt to elucidate the magnetic texture and its role in the switching process, we measured the magnetization dynamics in the presence of an external magnetic field. The measurements were still performed in a single-shot mode to avoid thermal accumulation in the sample. A magnetic field was continuously applied during each pump-probe event. The magnetic field was applied in two configurations relative to the sample surface: (i) in a purely out-of-plane direction and (ii) in a predominantly in-plane direction oriented at 35° to the sample surface with a smaller out-of-plane component. The dynamics observed for a purely out-of-plane applied field with a strength of 120 mT (not shown) were identical to the dynamics observed under zero applied field, within the limits of experimental resolution. The dynamics measured with a magnetic field applied partially in the sample plane are shown in Fig. 5 for three different field strengths of the in-plane component: 0 mT [row (a)], 118 mT [row (b)], and 185 mT [row (c)]. For the intermediate case with 118-mT in-plane field strength, the out-of-plane component of 83 mT was incapable of saturating the magnetization of the sample, whereas for a 185-mT in-plane field strength, the out-of-plane component (129 mT) was strong enough to saturate the magnetization of the sample into a monodomain state at its characteristic time scale. This lattermost experimental configuration is like that used by Tsema *et al.* [2] when studying Gd/FeCo multilayers. In those measurements, large-amplitude oscillations were observed in the dynamics.

When magnetization dynamics are excited under the highest in-plane field strength, a homogeneously reversed magnetic state is already attained within 50 ps. The ring textures seen in the zero-field dynamics between 20 and 70 ps are nearly absent for this case. Time-resolved quantitative

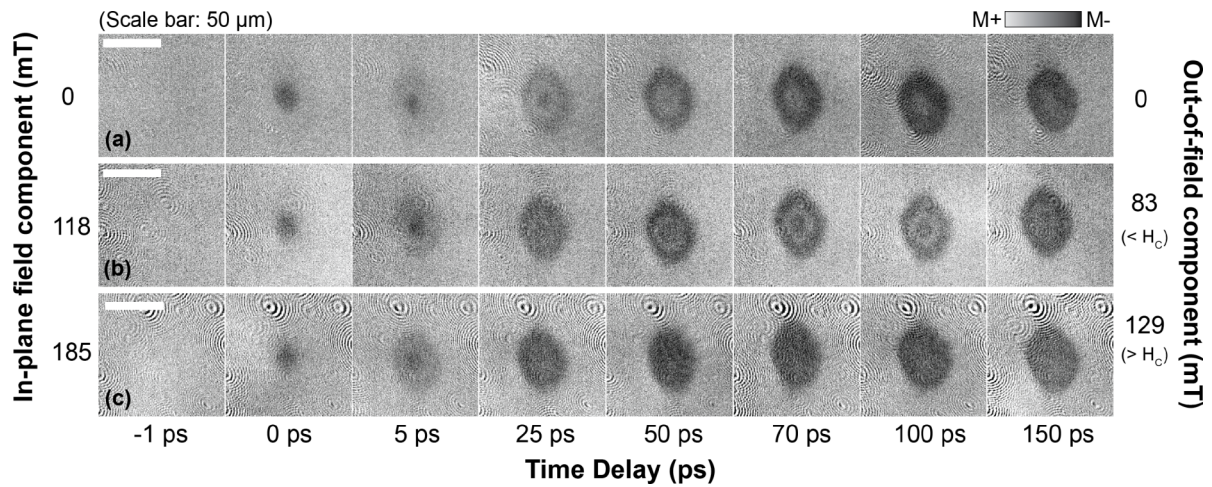


FIG. 5. Time-resolved magneto-optical images showing the temporal behavior of magnetization, measured for Tb(1.2 nm)/Co(1.8 nm) in the presence of an external magnetic field oriented 35° to the sample plane. The in-plane components of field strength are (a) 0 mT, (b) 118 mT, and (c) 185 mT. A pump fluence of 5.2 mJ/cm² was used.

traces extracted for the different ROIs are plotted in Fig. 6 for the three applied magnetic field strengths. With nonzero in-plane fields, an additional peak emerges in the slow demagnetization for all the ROIs at ~100 ps for 118-mT in-plane field strength and at ~60 ps for 185-mT in-plane

magnetic field strength. The frequency of this oscillationlike feature seems to increase upon increasing the strength of the applied magnetic field. Such a field dependence seems to indicate that this feature corresponds to magnetization precession, although more field-dependence data are needed

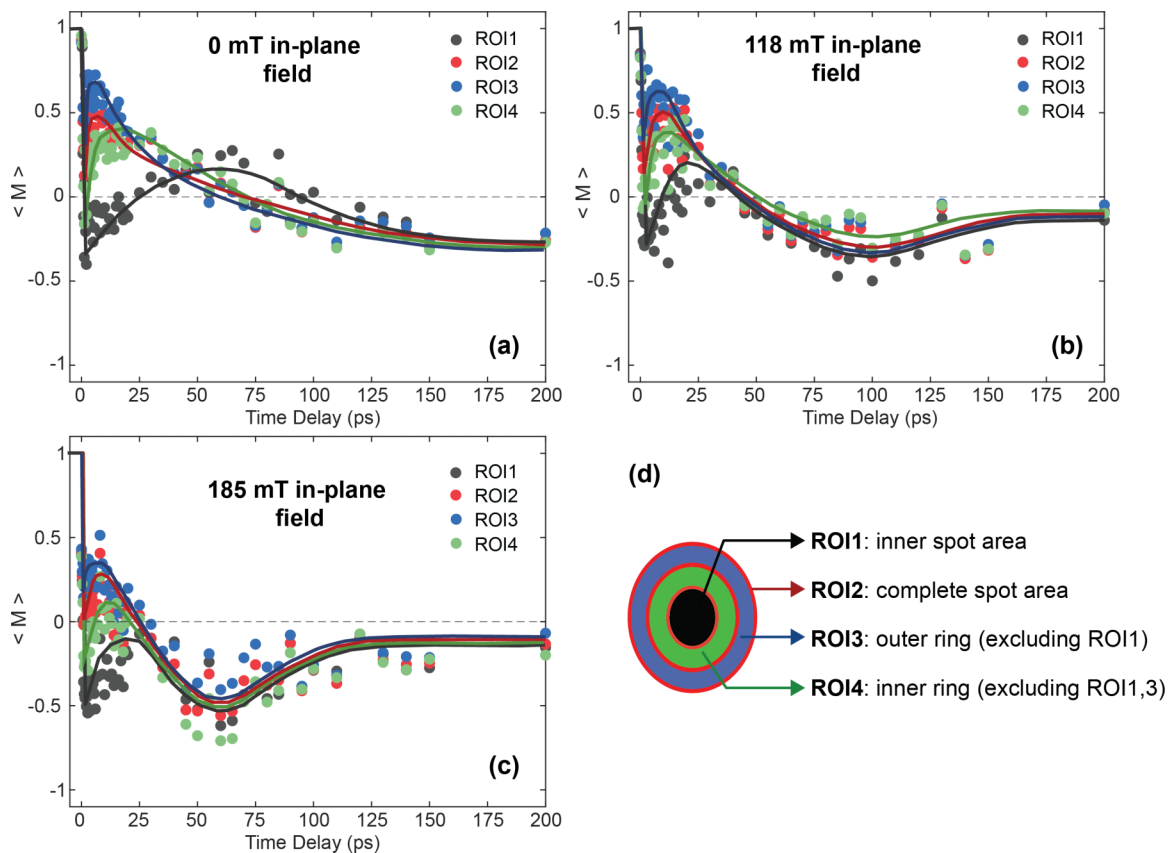


FIG. 6. Traces extracted from time-resolved magneto-optical images of laser-induced switching dynamics in the multilayer composition Tb(1.2 nm)/Co(1.8 nm) in the presence of an external magnetic field oriented 35° to the sample plane. The in-plane magnetic field component is of strengths (a) 0 mT, (b) 118 mT, and (c) 185 mT. The solid lines are guides to the eye. (d) A schematic of the different regions of interest (ROIs) used to obtain the traces shown in (a)–(c).

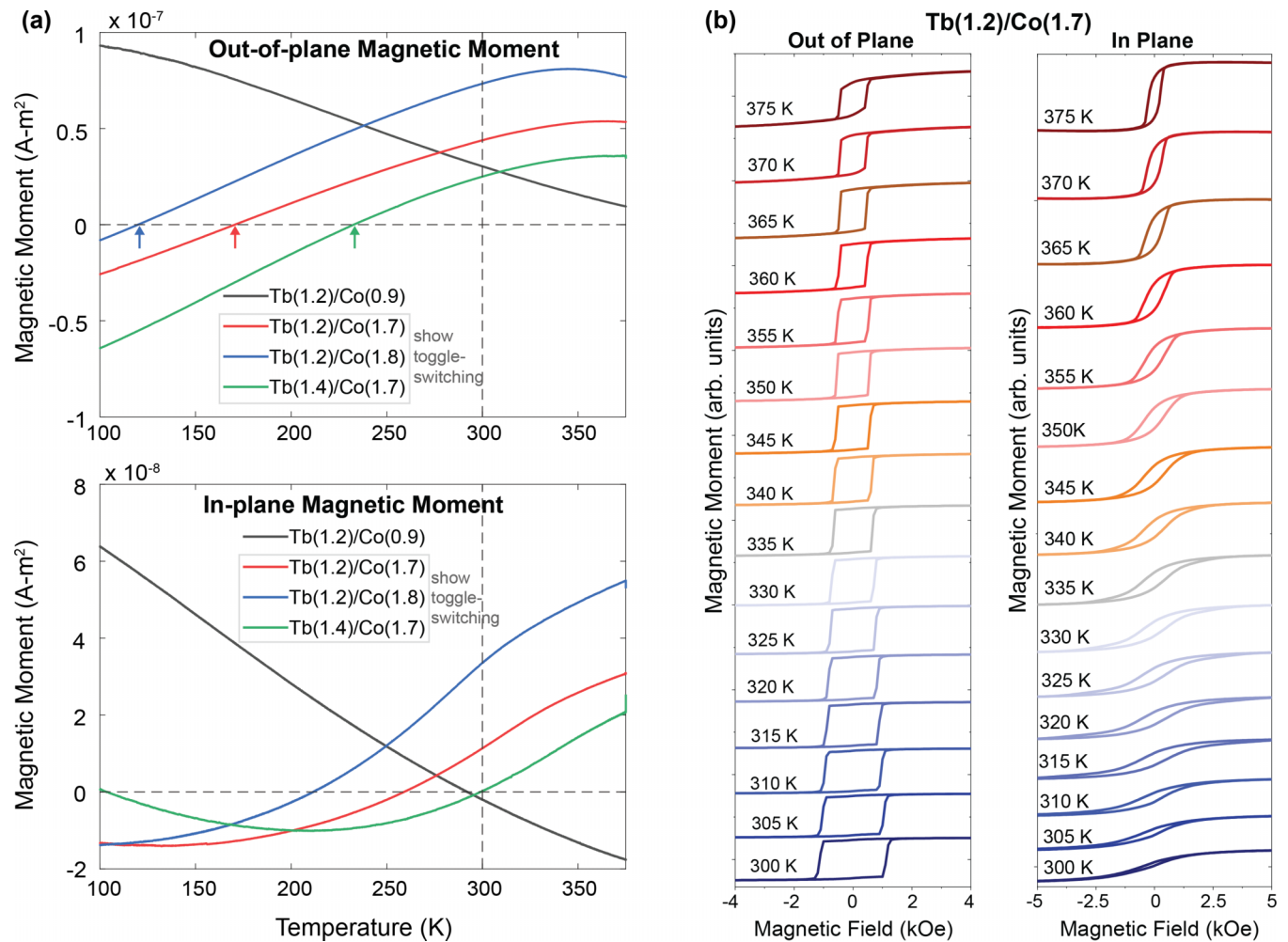


FIG. 7. (a) Temperature dependence of the out-of-plane magnetic moment measured under 200 mT applied field (top panel) and in-plane magnetic moment measured under 1 T applied field (bottom panel) for different compositions of the Tb/Co multilayers, measured using a superconducting quantum interference device vibrating sample magnetometer (SQUID-VSM). The colored arrows in the top panel indicate the compensation temperatures (T_{comp}) of each composition. (b) Evolution of the out-of-plane and in-plane magnetic hysteresis loops with increasing temperature from 300 K (loops at the bottom of the plots) to 375 K (loops at the top of the plots) for the composition Tb(1.2 nm)/Co(1.7 nm), showing an increasing in-plane component that emerges upon heating.

to confirm this conclusion. If this feature indeed corresponds to precessional dynamics, just a single period is observed for the peak in Tb/Co multilayers before the saturated switched state is stabilized. In comparison, in Gd/FeCo multilayers, multiple oscillation periods of ~ 140 ps (frequency 7.15 GHz) with a higher amplitude were observed [2]. This feature should arise from the action of the in-plane component of the applied magnetic field, as a purely out-of-plane magnetic field seems to not influence the dynamics. Although the field-induced precessional dynamics show similar magnetic texture as seen in the zero-field dynamics, the source of the effective magnetic field driving such precession for the zero-field case remains unclear. One possible origin for this effective field might emerge from a noncollinear canted magnetic state attained through a spin-flop transition, but hysteresis measurements in magnetic fields up to 8 T did not show any such transition. SQUID measurements of the temperature dependence of the in-plane and out-of-plane magnetic components for the samples, however, reveal nonzero in-plane

components of the magnetization for all compositions. For increasing temperatures, the in-plane hysteresis loops become squarer in shape, contrary to the out-of-plane hysteresis loops, which become less square shaped (Fig. 7), indicating a growing in-plane anisotropy with temperature. This might also somewhat explain the precessional dynamics, as the in-plane anisotropy that appears at higher temperatures could provide the in-plane effective magnetic field about which the magnetization precesses. Exploring the relationship between the layer thickness (i.e., composition) and the angular momentum compensation point could provide additional insights into the role of precessional dynamics on the switching.

Thus, detailed understanding of the ring textures and the spatially resolved single-shot switching dynamics remains incomplete. However, our reported dynamics in multilayers, combined with the proposed hypothesis on the differences between alloys and multilayers, point to some promising future directions to gain deeper understanding

of the dynamics in Tb-containing systems: namely, (i) determining the angular momentum compensation for the alloys and multilayers and correlating it with the switching behavior and (ii) studying the sublattice-resolved dynamics using x-ray probing techniques. Resolving the mechanism underlying the anomalous switching dynamics of the Tb/Co multilayers relative to the other single-shot switching systems in turn would lead to a more complete picture and routes for the optimization of single-shot switching in high anisotropy Tb-containing magnetic materials.

V. CONCLUSIONS AND OUTLOOK

Using pump-probe spectroscopy and microscopy, we have studied the time-resolved dynamics of single-shot switching of magnetization in Tb/Co multilayers. We have found that, supported by the general ideas on the behavior of RE angular momentum under the influence of crystal fields, multilayers are easier to switch with laser pulses. We have shown that the switched state stabilizes in ~ 100 ps, revealing a slower switching process that proceeds via a different pathway compared with the other reported single-shot switching systems such as (Gd,Fe)-based alloys and multilayers and RE-free $\text{Mn}_2\text{Ru}_x\text{Ga}$ Heusler alloys. The Co layer thickness affects the nature and time scale of the dynamics. Spatially resolved single-shot switching dynamics involves the formation and collapse of ring-shaped magnetic textures, the origin of which is still unclear but may involve precessional magnetization dynamics. The latter fact is yet another indication that the angular momentum compensation and predicted divergence of the effective gyromagnetic ratio are of crucial importance, given that the gyromagnetic ratio practically governs transverse motion of magnetization. The Tb/Co multilayer system is until now the only purely Tb-based RE-TM system showing robust and reproducible single-shot switching. Its rich temporal and spatial switching dynamics opens a broad scope for a deeper understanding of single-shot switching in general. Open questions remain related to the influence and role of Tb on the single-shot switching process and the absence of single-shot switching in alloys based on the very same magnetic constituents of Tb and Co.

ACKNOWLEDGMENTS

Part of this paper is supported by the Nederlandse Organisatie voor Wetenschappelijk Onderzoek (NWO), the European Union Horizon 2020 and the innovation programme under the FET-Open Grant Agreement No. 737093 (FEM-TOTERABYTE), and the European Research Council ERC Grant Agreement No. 856538 (3D MAGiC). This paper has received funding from the European Union's Horizon 2020 research and innovation program under FET-Open Grant Agreement No. 713481 (SPICE) and European Union's Horizon and under Marie Skłodowska-Curie Grant Agreement No. 861300 (COMRAD).

APPENDIX: TEMPERATURE DEPENDENCE OF MAGNETIZATION IN Tb/Co

Using a SQUID vibrating sample magnetometer (VSM), we measured the static temperature dependence of magnetization in different Tb/Co multilayered stacks. The top panel of Fig. 7(a) shows the out-of-plane magnetic moment for various Tb/Co heterostructures, measured under an applied out-of-plane magnetic field of 200 mT strength. The bottom panel shows the in-plane magnetic moment measured under an applied in-plane magnetic field of 1 T strength. From Fig. 7(a), we observe that the three samples that exhibit single-shot switching have a T_{comp} [marked with arrows] lying below RT. In contrast, the sample that does not exhibit single-shot switching has a compensation point above RT. Moreover, we note that the samples generally have a magnetic moment aligned both in and out of the sample plane.

In Fig. 7(b), we present hysteresis loops for $[\text{Tb}(1.2\text{ nm})/\text{Co}(1.7\text{ nm})]_5$ measured with the applied field oriented out-of-plane (left column) and in-plane (right column), at various temperatures. In general, we observe that, as the temperature increases from RT, the out-of-plane coercive field decreases while the hysteresis loop becomes less square. In contrast, for the in-plane measurements, we observe that the magnetic moment increases with temperature, while the hysteresis loop becomes more squarelike. This agrees with the measurements shown in Fig. 7(a). The reason for this behavior is unclear.

-
- [1] T. A. Ostler, J. Barker, R. F. L. Evans, R. W. Chantrell, U. Atxitia, O. Chubykalo-Fesenko, S. El Moussaoui, L. Le Guyader, E. Mengotti, L. J. Heyderman *et al.*, Ultrafast heating as a sufficient stimulus for magnetization reversal in a ferrimagnet, *Nat. Commun.* **3**, 666 (2012).
- [2] Y. Tsema, Laser Induced Magnetization Dynamics and Switching in Multilayers, Ph.D. Thesis, Radboud University Nijmegen, 2017.
- [3] M. L. M. Laliou, M. J. G. Peeters, S. R. R. Haenen, R. Lavrijsen, and B. Koopmans, Deterministic all-optical switching of synthetic ferrimagnets using single femtosecond laser pulses, *Phys. Rev. B* **96**, 220411(R) (2017).
- [4] C. Banerjee, N. Teichert, K. E. Siewierska, Z. Gercsi, G. Y. P. Atcheson, P. Stamenov, K. Rode, J. M. D. Coey, and J. Besbas, Single pulse all-optical toggle switching of magnetization without gadolinium in the ferrimagnet $\text{Mn}_2\text{Ru}_x\text{Ga}$, *Nat. Commun.* **11**, 4444 (2020).
- [5] A. Ceballos, A. Pattabi, A. El-Ghazaly, S. Ruta, C. P. Simon, R. F. L. Evans, T. Ostler, R. W. Chantrell, E. Kennedy, M. Scott *et al.*, Role of element-specific damping in ultrafast, helicity-independent, all-optical switching dynamics in amorphous (Gd,Tb)Co thin films, *Phys. Rev. B* **103**, 024438 (2021).
- [6] L. Avilés-Félix, A. Olivier, G. Li, C. S. Davies, L. Álvaro-Gómez, M. Rubio-Roy, S. Auffret, A. Kirilyuk, A. V. Kimel, Th. Rasing *et al.*, Single-shot all-optical switching of magnetization in Tb/Co multilayer-based electrodes, *Sci. Rep.* **10**, 5211 (2020).
- [7] L. Avilés-Félix, L. Álvaro-Gómez, G. Li, C. S. Davies, A. Olivier, M. Rubio-Roy, S. Auffret, A. Kirilyuk, A. V. Kimel, Th. Rasing *et al.*, Integration of Tb/Co multilayers within

- optically switchable perpendicular magnetic tunnel junctions, *AIP Adv.* **9**, 125328 (2019).
- [8] M. Finazzi, M. Savoini, A. R. Khorsand, A. Tsukamoto, A. Itoh, L. Duò, A. Kirilyuk, Th. Rasing, and M. Ezawa, Laser-Induced Magnetic Nanostructures with Tunable Topological Properties, *Phys. Rev. Lett.* **110**, 177205 (2013).
- [9] R. Moreno, T. A. Ostler, R. W. Chantrell, and O. Chubykalo-Fesenko, Conditions for thermally induced all-optical switching in ferrimagnetic alloys: Modeling of TbCo, *Phys. Rev. B* **96**, 014409 (2017).
- [10] S. Alebrand, M. Gottwald, M. Hehn, D. Steil, M. Cinchetti, D. Lacour, E. E. Fullerton, M. Aeschlimann, and S. Mangin, Light-induced magnetization reversal of high-anisotropy TbCo alloy films, *Appl. Phys. Lett.* **101**, 162408 (2012).
- [11] S. Mangin, M. Gottwald, C-H. Lambert, D. Steil, V. Uhlř, L. Pang, M. Hehn, S. Alebrand, M. Cinchetti, G. Malinowski *et al.*, Engineered materials for all-optical helicity-dependent magnetic switching, *Nat. Mater.* **13**, 286 (2014).
- [12] M. S. El Hadri, P. Pirro, C-H. Lambert, S. Petit-Watlot, Y. Quessab, M. Hehn, F. Montaigne, G. Malinowski, and S. Mangin, Two types of all-optical magnetization switching mechanisms using femtosecond laser pulses, *Phys. Rev. B* **94**, 064412 (2016).
- [13] B. Hebler, A. Hassdenteufel, P. Reinhardt, H. Karl, and M. Albrecht, Ferrimagnetic Tb-Fe alloy thin films: Composition and thickness dependence of magnetic properties and all-optical switching, *Front. Mater.* **3**, 8 (2016).
- [14] A. Ciuciulkaite, K. Mishra, M. V. Moro, I-A. Chioar, R. M. Rowan-Robinson, S. Parchenko, A. Kleibert, B. Lindgren, G. Andersson, C. S. Davies *et al.*, Magnetic and all-optical switching properties of amorphous Tb_xCo_{100-x} alloys, *Phys. Rev. Mater.* **4**, 104418 (2020).
- [15] C. S. Davies, G. Bonfiglio, K. Rode, J. Besbas, C. Banerjee, P. Stamenov, J. M. D. Coey, A. V. Kimel, and A. Kirilyuk, Exchange-driven all-optical magnetic switching in compensated 3d ferrimagnets, *Phys. Rev. Res.* **2**, 032044(R) (2020).
- [16] K. Vahaplar, A. M. Kalashnikova, A. V. Kimel, D. Hinzke, U. Nowak, R. Chantrell, A. Tsukamoto, A. Itoh, A. Kirilyuk, and Th. Rasing, Ultrafast Path for Optical Magnetization Reversal Via a Strongly Nonequilibrium State, *Phys. Rev. Lett.* **103**, 117201 (2009).
- [17] M. Beens, M. L. M. Laliu, A. J. M. Deenen, R. A. Duine, and B. Koopmans, Comparing all-optical switching in synthetic-ferrimagnetic multilayers and alloys, *Phys. Rev. B* **100**, 220409(R) (2019).
- [18] C. S. Davies, T. Janssen, J. H. Mentink, A. Tsukamoto, A. V. Kimel, A. F. G. van der Meer, A. Stupakiewicz, and A. Kirilyuk, Pathways for Single-Shot All-Optical Switching of Magnetization in Ferrimagnets, *Phys. Rev. Appl.* **13**, 024064 (2020).
- [19] C. S. Davies, J. H. Mentink, A. V. Kimel, Th. Rasing, and A. Kirilyuk, Helicity-independent all-optical switching of magnetization in ferrimagnetic alloys, *J. Magn. Magn. Mater.* **563**, 169851 (2022).
- [20] R. K. Wangsness, Sublattice effects in magnetic resonance, *Phys. Rev.* **91**, 1085 (1953).
- [21] C. Kittel, Theory of ferromagnetic resonance in rare earth garnets. I. *g* values, *Phys. Rev.* **115**, 1587 (1959).
- [22] J. H. van Vleck, Primitive theory of ferrimagnetic resonance frequencies in rare-earth iron garnets, *Phys. Rev.* **123**, 58 (1961).
- [23] I. Radu, K. Vahaplar, C. Stamm, T. Kachel, N. Pontius, H. A. Dürr, T. A. Ostler, J. Barker, R. F. L. Evans, R. W. Chantrell *et al.*, Transient ferromagnetic-like state mediating ultrafast reversal of antiferromagnetically coupled spins, *Nature (London)* **472**, 205 (2011).
- [24] J. H. Mentink, J. Hellsvik, D. V. Afanasiev, B. A. Ivanov, A. Kirilyuk, A. V. Kimel, O. Eriksson, M. I. Katsnelson, and Th. Rasing, Ultrafast Spin Dynamics in Multisublattice Magnets, *Phys. Rev. Lett.* **108**, 057202 (2012).
- [25] G. P. Rodrigue, H. Meyer, and R. V. Jones, Resonance measurements in magnetic garnets, *J. Appl. Phys.* **31**, S376 (1960).
- [26] N. Ohta, T. Ikeda, F. Ishida, and Y. Sugita, High *g* bubble garnets without containing Eu³⁺ ion, *J. Phys. Soc. Jpn.* **43**, 705 (1977).
- [27] V. V. Randoshkin and V. B. Sigachev, Experimental test of the one-dimensional theory of motion of domain walls in uniaxial ferromagnets, *Pis'ma Zh. Eksp. Teor. Fiz.* **42**, 34 (1985).
- [28] M. V. Logunov, S. S. Safonov, A. S. Fedorov, A. A. Danilova, N. V. Moiseev, A. R. Safin, S. A. Nikitov, and A. Kirilyuk, Domain Wall Motion Across Magnetic and Spin Compensation Points in Magnetic Garnets, *Phys. Rev. Appl.* **15**, 064024 (2021).
- [29] T. Miyadai, Ferrimagnetic resonance in europium-iron garnet, *J. Phys. Soc. Jpn.* **15**, 2205 (1960).
- [30] B. Johnson and R. S. Tebble, The infra-red Faraday effect and *g* values in rare-earth garnets, *Proc. Phys. Soc.* **87**, 935 (1966).
- [31] C. M. Srivastava, B. Uma Maheshwar Rao, and N. S. Hanumantha Rao, Magnetic relaxation in rare earth garnets, *Bull. Mater. Sci.* **7**, 237 (1985).
- [32] T. K. Wagner and J. L. Stanford, Observation of magneto-elastic effects in terbium metal by ferromagnetic resonance at $\lambda = 2.5-3$ mm, *Phys. Rev.* **184**, 505 (1969).
- [33] L. W. Hart and J. L. Stanford, Free-Lattice-Model Ferromagnetic Resonance in Terbium at 24 GHz, *Phys. Rev. Lett.* **27**, 676 (1971).
- [34] D. T. Vigen and S. H. Liu, Long-Wavelength Magnons in Heavy Rare Earths: Free or Frozen Lattice? *Phys. Rev. Lett.* **27**, 674 (1971).
- [35] K. Mishra, Towards Nanoscale Confinement of All Optical Magnetization Switching, Ph.D. Thesis, Radboud University Nijmegen, 2022.
- [36] A. Mekonnen, A. R. Khorsand, M. Cormier, A. V. Kimel, A. Kirilyuk, A. Hrabec, L. Ranno, A. Tsukamoto, A. Itoh, and Th. Rasing, Role of the inter-sublattice exchange coupling in short-laser-pulse-induced demagnetization dynamics of GdCo and GdCoFe alloys, *Phys. Rev. B* **87**, 180406(R) (2013).
- [37] Z. Chen, S. Li, S. Zhou, and T. Lai, Ultrafast dynamics of 4*f* electron spins in TbFeCo film driven by inter-atomic 3*d*-5*d*-4*f* exchange coupling, *New. J. Phys.* **21**, 123007 (2019).
- [38] K. Vahaplar, A. M. Kalashnikova, A. V. Kimel, S. Gerlach, D. Hinzke, U. Nowak, R. Chantrell, A. Tsukamoto, A. Itoh, A. Kirilyuk *et al.*, All-optical magnetization reversal by circularly polarized laser pulses: Experiment and multiscale modeling, *Phys. Rev. B* **85**, 104402 (2012).
- [39] M. Djordjevic and M. Münzenberg, Connecting the timescales in picosecond remagnetization experiments, *Phys. Rev. B* **75**, 012404 (2007).
- [40] T. Roth, A. J. Schellekens, S. Alebrand, O. Schmitt, D. Steil, B. Koopmans, M. Cinchetti, and M. Aeschlimann, Temperature Dependence of Laser-Induced Demagnetization in Ni: A Key

- for Identifying the Underlying Mechanism, *Phys. Rev. X* **2**, 021006 (2012).
- [41] C. S. Davies, K. H. Prabhakara, M. D. Davydova, K. A. Zvezdin, T. B. Shapaeva, S. Wang, A. K. Zvezdin, A. Kirilyuk, Th. Rasing, and A. V. Kimel, Anomalous Damped Heat-Assisted Route for Precessional Magnetization Reversal in an Iron Garnet, *Phys. Rev. Lett.* **122**, 027202 (2019).
- [42] A. R. Khorsand, M. Savoini, A. Kirilyuk, A. V. Kimel, A. Tsukamoto, A. Itoh, and Th. Rasing, Element-Specific Probing of Ultrafast Spin Dynamics in Multisublattice Magnets with Visible Light, *Phys. Rev. Lett.* **110**, 107205 (2013).
- [43] C. E. Graves, A. H. Reid, T. Wang, B. Wu, S. de Jong, K. Vahaplar, I. Radu, D. P. Bernstein, M. Messerschmidt, L. Müller *et al.*, Nanoscale spin reversal by non-local angular momentum transfer following ultrafast laser excitation in ferrimagnetic GdFeCo, *Nat. Mater.* **12**, 293 (2013).